INT. J. NUM. METH. HEAT FLUID FLOW, VOL. 5, 615–627 (1995)

EFFECTS OF VARIABLE PROPERTY AND SURFACE RADIATION ON LAMINAR NATURAL CONVECTION IN A SQUARE ENCLOSURE

SWARNENDU SEN AND A. SARKAR

Application Software R & D Laboratory, Department of Mechanical Engineering, Jadavpur University, Calcutta 700032, India

ABSTRACT

The interaction of variable property convection and surface radiation in a differentially heated square cavity is considered. Effect of surface radiation on natural convection has been studied from the point of view of flow structure and isotherm patterns. Wherever possible, a comparative study has been invoked between the outcome of the present work and the constant property formulation. The finite element method has been used in the present work and associated formulation schemes have been described in detail.

KEY WORDS Finite element Natural convection Laminar flow Variable property Surface radiation

NOMENCLATURE

u, v	fluid velocities,
U, V	non-dimensional fluid velocities,
H	cavity height,
U_0	characteristic velocity $[=\sqrt{\beta_r g H(T_H - T_C)}]$
T_H, T_C	hot and cold wall temperature,
T_r	reference temperature
g	acceleration due to gravity,
c	specific heat,
c_r	specific heat at reference temperature,
c^*	non-dimensional specific heat $[= c/c_r]$,
k	thermal conductivity,
k_r	thermal conductivity at reference temperature
k^*	non-dimensional thermal conductivity $[= k/k_r]$,
p	fluid pressure,
p_r	reference pressure,
p^*	non-dimensional pressure $[= p/p_r]$,
Pr_r	reference Prandtl number $[= \nu_r/\alpha_r]$,
Gr_r	reference Grashoff number $[= g\beta_r(T_H - T_C)H^3/\nu_r^2]$,
J	Radiosity,
J^*	non-dimensional radiosity $[= J/\sigma T_H^4]$,
F_{ij}	view-factor of ith surface from jth surface,
RC	radiation–conduction parameter $[= H\sigma T_H^4/k_r(T_H - T_C)]$,
TTD	terminal temperature difference $[= T_H - T_C]$,
N	number of participating surfaces; also shape function,
Nu_H	hot wall Nusselt number,
Nu_C	cold wall Nusselt number,
Q_H	net heat transfer at hot wall,
Q_{con_H}	convective heat transfer at hot wall,
Q_{rad_H}	radiative heat transfer at hot wall,
Q_C	net heat transfer at cold wall,
Q_{con_C}	convective heat transfer at cold wall,
Q_{rad_C}	radiative heat transfer at cold wall.

Greek symbols

β_r	coefficient of volume expansion at reference temperature,
θ	non-dimensional temperature $[= (T - T_r)/(T_H - T_C)]$,
ρ	fluid density,
ρ_r	fluid density at reference temperature,
ρ^*	non-dimensional fluid density $[= \rho/\rho_r]$,
μ	fluid viscosity,

0961–5539/95/070615–13$2.00

Received August 1993
Revised May 1994

μ_r fluid viscosity at reference temperature,
μ^* non-dimensional fluid viscosity $[= \mu/\mu_r]$,
σ Stephan–Boltzman constant,
ε_i emissivity of ith surface,
α_r thermal diffusivity at reference temperature,
ν_r kinematic viscosity at reference temperature.

INTRODUCTION

Natural convection is a matter of considerable research interest due to its direct relevance in a variety of applications ranging from growth of crystals, solar collector performance, fire and smoke spread in rooms to large-scale geophysical phenomena. With the advent of high speed digital computers, research interest was shifted towards numerical simulation of these situations; consequently, robust computer programs have been developed and tested with benchmark solution[1] before they can be used for simulating real life situations. The benchmark solution is based on the assumptions of steady, two-dimensional, incompressible natural convection in a differentially heated square cavity. Since then, a considerable amount of research work has been reported and many of them have contributed greatly towards understanding the physics behind natural convection; however, some simplifications, such as universal adoption of Boussinesq approximation, have often eluded the scientific community from gaining further insight of the subject. It is generally known that this approximation is valid for small temperature differences. As thermal conditions became severe in some specialized application areas, it appeared that a more realistic approach will result if the effect of variable property was taken into account. Polezhaev[2] was an early investigator in this field who reported the numerical solution of the full scale variable property problem over a Grashoff number range between 5×10^3 to 10^6. Macgregor and Emery[3] employed Boussinesq approximation along with variable viscosity and thermal conductivity in their work which worked well for liquid. Subsequently, Leonardi and Reizes[4,5] discussed at length the numerical scheme which they employed as also the effect of overheat ratio on the flow structure and isotherm patterns for the case of variable property convection in enclosures. Zhong *et al.*[6] addressed several important problems, associated with variable property convection, such as the reference temperature issue and the limits of Boussinesq approximation. In their work, the reference property values are based on cold wall temperature. They also concluded that the Boussinesq approximation was generally valid when the overheat ratio was less than 0.1. The effect of the variable fluid properties on laminar free convection heat transfer of monoatomic gas, polyatomic gas, air and water vapour along an isothermal vertical flat plate has been reported by Shang and Wang[7,8]. They noted that for polyatomic gases the classical Boussinesq approximation did not hold good even for small ranges of overheat ratio. Subsequent to these observations, it was soon realised that besides the variable property effect, the interaction of natural convection with radiation may have a significant role in some thermal systems where a large overall temperature difference exists. In many natural convection processes, the radiative heat transfer may affect the temperature field and consequently the flow field through absorption and emission processes within the fluid. This effect may be negligibly small if the fluid is dry air. However, the emission of radiation by the boundaries may have an important bearing on the boundary temperatures. Because of the coupling between the thermal and flow fields through buoyancy effects, the changes in boundary temperatures caused by radiative transfer may exercise a stronger influence than expected. However, in spite of its wide applications, the interaction analysis did not receive adequate attention. In fact Zhong *ét al.*[6] very recently pointed out the necessity of solving the coupled heat transfer problems. However, a few case studies are found in which the combined heat transfer problem has been addressed[9–12]. Lauriat[13] considered convection in an insulated enclosure, including the effect of long wave radiation. Behnia *et al.*[14] carried out a numerical investigation to study the effect of combined natural convection and radiation on the flow pattern and heat transfer in a rectangular, two-dimensional cavity containing a non-participating fluid. In their study, the terminal

temperature difference was 130°C and the Rayleigh number was varied between 10^4 to 3×10^5. In spite of a large overheat ratio, a constant property fluid with Boussinesq approximation was used to model the convection in their study.

From the review of the above referred literature, it is recognised that a benchmark solution for compressible fluid flow in an enclosure does not exist. Moreover, a systematic investigation of the interaction of radiation with variable property convection has not been reported. The objective of the present work is, therefore, to carry out an extensive numerical investigation on such interactions under extreme thermal conditions. The differentially heated square cavity has been chosen as the physical domain. The Rayleigh number was varied between 10^3 to 4×10^7 while the difference in hot and cold wall temperatures was of the order of 700°C. Finite element method has been employed as the numerical tool in the present work.

GOVERNING EQUATIONS AND BOUNDARY CONDITIONS

For a steady, two-dimensional, variable property Newtonian fluid, the conservation equations may be expressed as follows:

$$\frac{\partial(\rho u)}{\partial x} + \frac{\partial(\rho v)}{\partial y} = 0 \tag{1a}$$

$$\rho\left(u\frac{\partial u}{\partial x} + v\frac{\partial u}{\partial y}\right) = -\frac{\partial p}{\partial x} + \frac{\partial}{\partial x}\left[2\mu\frac{\partial u}{\partial x} - \frac{2\mu}{3}\left(\frac{\partial u}{\partial x} + \frac{\partial v}{\partial y}\right)\right] + \frac{\partial}{\partial y}\left[\mu\left(\frac{\partial u}{\partial y} + \frac{\partial v}{\partial x}\right)\right] \tag{1b}$$

$$\rho\left(u\frac{\partial v}{\partial x} + v\frac{\partial v}{\partial y}\right) = -\frac{\partial p}{\partial y} + \frac{\partial}{\partial y}\left[2\mu\frac{\partial v}{\partial y} - \frac{2\mu}{3}\left(\frac{\partial u}{\partial x} + \frac{\partial v}{\partial y}\right)\right] + \frac{\partial}{\partial x}\left[\mu\left(\frac{\partial u}{\partial y} + \frac{\partial v}{\partial x}\right)\right] - \rho g \tag{1c}$$

and

$$\frac{\partial}{\partial x}(\rho c u T) + \frac{\partial}{\partial y}(\rho c v T) = \frac{\partial}{\partial x}\left(k\frac{\partial T}{\partial x}\right) + \frac{\partial}{\partial y}\left(k\frac{\partial T}{\partial y}\right) \tag{1d}$$

In (1d), the effect of viscous dissipation and the work of compression has been neglected. Equations (1a)–(1d) are non-dimensionalized with the help of the following reference quantities:

$$X = x/H; \quad Y = y/H; \quad u_0 = \sqrt{\beta_r g H (T_H - T_C)}; \quad \rho^* = \rho/\rho_r; \quad P^* = \frac{p - p_r}{\rho_r u_0^2}$$

$$\mu^* = \mu/\mu_r; \quad c^* = c/c_r; \quad k^* = k/k_r; \quad Pr_r = \nu_r/\alpha_r; \quad \theta = \frac{T - T_r}{T_H - T_C}; \quad U = u/u_0; \quad V = v/u_0$$

Quantities with subscript r refer to the property values at the reference temperature. Throughout the present work, the cold wall temperature has been assumed to be the reference temperature. With the introduction of the above-mentioned non-dimensional quantities into (1a)–(1d), one obtains the following system of equations:

$$\frac{\partial(\rho^* U)}{\partial X} + \frac{\partial(\rho^* V)}{\partial Y} = 0 \tag{2a}$$

$$\rho^*\left(U\frac{\partial U}{\partial X} + V\frac{\partial U}{\partial Y}\right) = -\frac{\partial P}{\partial X} + \frac{1}{\sqrt{Gr_r}}\frac{\partial}{\partial X}\left[2\mu^*\frac{\partial U}{\partial X} - \frac{2\mu^*}{3}\left(\frac{\partial U}{\partial X} + \frac{\partial V}{\partial Y}\right)\right] + \frac{1}{\sqrt{Gr_r}}\frac{\partial}{\partial Y}\left[\mu^*\left(\frac{\partial U}{\partial Y} + \frac{\partial V}{\partial X}\right)\right] \tag{2b}$$

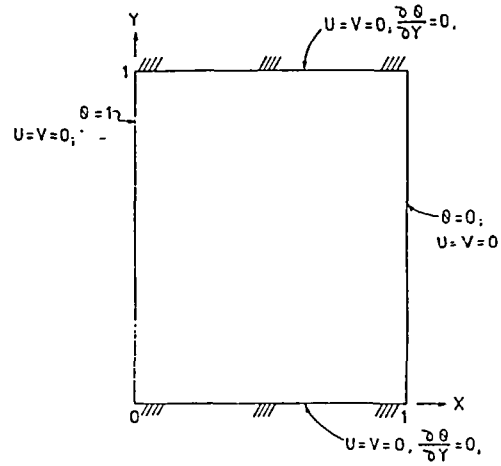

Figure 1 Test computational domain

$$\rho^*\left(U\frac{\partial V}{\partial X}+V\frac{\partial V}{\partial Y}\right)=-\frac{\partial P}{\partial Y}+\frac{1}{\sqrt{Gr_r}}\frac{\partial}{\partial Y}\left[2\mu^*\frac{\partial V}{\partial Y}-\frac{2\mu^*}{3}\left(\frac{\partial U}{\partial X}+\frac{\partial V}{\partial Y}\right)\right]$$
$$+\frac{1}{\sqrt{Gr_r}}\frac{\partial}{\partial X}\left[\mu^*\left(\frac{\partial U}{\partial Y}+\frac{\partial V}{\partial X}\right)\right]+\theta \tag{2c}$$

and

$$\frac{\partial}{\partial X}(\rho^*c^*U\theta)+\frac{\partial}{\partial Y}(\rho^*c^*V\theta)=\frac{1}{Pr_r\sqrt{Gr_r}}\frac{\partial}{\partial X}\left(k^*\frac{\partial\theta}{\partial x}\right)+\frac{\partial}{\partial Y}\left(k^*\frac{\partial\theta}{\partial Y}\right) \tag{2d}$$

It may be noted that the body force term in (2c) is based on the difference between the local fluid density and the density corresponding to fluid hydrostatic equilibrium condition. Finally, the boundary conditions are described in *Figure 1*. However, when surface radiation is to be considered the thermal boundary conditions at the insulated walls are modified as described below: As it has been assumed that the medium is not participating, the radiation phenomena will be limited to the boundary surfaces only. For pure convection cases, one substitutes, for adiabatic surfaces, $-k(\partial T/\partial y)=0$. This needs to be slightly modified in the presence of surface radiation. The specification of boundary condition on the adiabatic surface is completed by equating the convective and radiative transfers on the plate as shown below:

$$-k\left.\frac{\partial T}{\partial y}\right|_{\text{ith surface}}=J_i-\sum_{j=1}^{N}F_{ij}J_j$$

Introducing non-dimensional quantities, the above boundary condition can be transformed in the following form:

$$k^*\frac{\partial\theta}{\partial Y}=RC\left[\sum_{j=1}^{N}F_{ij}J_j^*-J_i^*\right] \tag{3}$$

where $RC\ [=H\sigma T_H^4/k_r(T_H-T_C)]$ is the radiation–conduction parameter and $J^*=J/\sigma T_H^4$.

Equation (3) constitutes the gradient of the boundary condition for the energy equation (2d). Throughout the present work, the participating surfaces are assumed to be grey.

FINITE ELEMENT FORMULATION AND METHOD OF SOLUTION

Standard Galerkin formulation has been employed throughout the present work. However, some simplifying assumptions had to be made during the course of discretization as illustrated below: For example, let us consider the discretization of (2d):

$$F_4 = \int N^T\left[\frac{\partial}{\partial X}(\rho^* c^* U\theta) + \frac{\partial}{\partial Y}(\rho^* c^* V\theta)\right] dA^{(e)}$$

$$- \int N^T \frac{1}{Pr_r\sqrt{Gr_r}}\left[\frac{\partial}{\partial X}\left(k^* \frac{\partial\theta}{\partial X}\right) + \frac{\partial}{\partial Y}\left(k^* \frac{\partial\theta}{\partial Y}\right)\right] dA^{(e)}$$

It has been assumed that the properties remain constant element wise. This assumption permits the negligence of the spatial variation of the property values while computing the element stiffness matrix. So (2d) may be recast as:

$$F_4 = \rho^{*(e)} c^{*(e)} \int N^T\left[\frac{\partial}{\partial X}(U\theta) + \frac{\partial}{\partial Y}(V\theta)\right] dA^{(e)} - \frac{1}{Pr\sqrt{Gr_r}} k^{*(e)} \int N^T\left[\frac{\partial^2\theta}{\partial X^2} + \frac{\partial^2\theta}{\partial Y^2}\right] dA^{(e)}$$

While computing the property values $\rho^{*(e)}$, $c^{*(e)}$, $k^{*(e)}$ or $\mu^{*(e)}$, as the case may be, the temperature at the point ($\xi = \eta = 0$) is computed; subsequently, the property values are interpolated (corresponding to this temperature) from Reference 15.

The rest of the discretization scheme is analogous to the conventional methods of treating incompressible flow in which the non-linearities are treated by the Newton–Raphson method and the resulting simultaneous equations are solved by Frontal solver. Detail of the method has been described elsewhere[16]. Convergence of the solution is assumed to be achieved when the largest residue is below a pre-assigned value, as low as 10^{-9} for pure convection cases. However, when radiation is present, this limit has to be raised to 10^{-8} due to slower convergence rate. During iterative process, (2a) to (2d) are solved first and the temperature distribution of the adiabatic surfaces are obtained. Subsequently, the following non-dimensional radiosity equations are solved:

$$J_i^* - (1 - \varepsilon_i) \sum_{j=1}^{N} J_{ij}^* = \varepsilon_i (T_i/T_H)^4 \tag{4}$$

where N denotes the number of discretized participating surfaces. For isothermal surfaces, T_i assumes the values of T_H or T_C depending on its location. When the ith side corresponds to an adiabatic surface, the average temperature of that side of the element is considered.

Subsequent to the solution of (4), the Navier–Stokes and energy are solved once again; but this time (3) is considered as a boundary condition. The scheme is subsequently repeated. However, during two successive iterations the radiosity values are averaged.

It has been observed that the number of iterations are much more in the presence of radiation. For example, when pure convection is present, only six to seven iterations are necessary when one moves from Rayleigh number 10^6 to 10^7; whereas around twenty iterations are required under the same condition when radiation is present.

During the course of iteration the temperature of the isothermal walls (T_H, T_C) and emissivity has been supplied as the input. From the value of the cold wall temperature, the reference property values are obtained including the reference Prandtl number (Pr_r). For a specific Rayleigh number, the characteristic dimension of the cavity (H) may be calculated. From this value of the cavity dimension, the reference value of the velocity (U_0) can be calculated. So, for a specific case of Rayleigh number, the value of U_0 and H change. The value of H is required in the computation of total energy transfer across isothermal walls. The convective heat transfer from

the hot wall can be calculated as:

$$Q_{\text{con}_H} = -k_r H(T_H - T_C)\int_0^1 k^* \frac{\partial \theta}{\partial X}\,\mathrm{d}Y$$

The radiative transfer from a segment i on the isothermal surface can be calculated as:

$$q_{\text{rad}_i} = \left(J_i^* - \sum_{j=1}^{N} J_j^* F_{ij}\right)\sigma T_H^4$$

RESULTS AND DISCUSSION

Before a detail discussion on the combined mode heat transfer can be initiated, a brief discussion on grid independence study is necessary. In the present study, the mesh size is indicated by ($M \times N$) in which M stands for the number of elements in X-direction and N for the same along Y-direction. The grid independence study starts with a relatively coarse-size mesh (14 × 14). It may be noted that an eight-noded isoparametric element has been employed throughout the present work for the discretization of the computational domain. The mesh, in subsequent studies have been continuously refined up to a size of (30 × 14). The number of elements in the Y-direction had to be limited to 14, in order to restrain the size of the front width. Secondly, it has been observed that the thermal gradients are predominantly along the X-direction at either of the active walls. These lead to the fact that it is more demanding to increase the number of elements in X-direction than Y-direction. The grid independence study starts with the effect of variable property convection and the detailed results are indicated in *Tables 1a* and *2a*. While the value of the cold wall temperature was kept constant at 300 K, the hot wall temperature was assigned values 500 K and 1000 K. As is evident in both these Tables, there is a considerable difference in the heat balances of hot and cold walls at lower mesh sizes and this difference significantly narrows down as the mesh size is increased. This disagreement of energy balances at the active walls is typical of variable property convection only but, surprisingly, it has not

Table 1a Grid independence study for convection (T_H = 500 K, T_C = 300 K, $Ra = 10^7$, $Pr_r = 0.71$)

Grid	Nu_H	Nu_C	Q_H (W)	Q_C (W)
14 × 14	18.09	16.43	94.96	86.25
18 × 14	17.76	16.67	93.28	87.50
22 × 14	17.60	16.88	92.36	88.61
26 × 14	17.50	17.05	91.83	89.46
30 × 14	17.45	17.14	91.57	89.96

Table 1b Grid independence study for convection–radiation interaction (T_H = 500 K, T_C = 300 K, $Ra = 10^7$, $Pr_r = 0.71$, $\varepsilon = 0.1$)

Grid	Q_{con_H} (W)	Q_{rad_H} (W)	Q_H (W)	Q_{con_C} (W)	Q_{rad_C} (W)	Q_C (W)
14 × 14	88.30	15.22	103.52	83.40	12.47	95.87
18 × 14	87.22	15.30	102.52	84.57	12.40	96.97
22 × 14	86.76	15.35	102.11	85.61	12.34	97.95
26 × 14	86.61	15.36	101.97	86.52	12.33	98.85
30 × 14	86.67	15.36	102.03	87.16	12.34	99.50

Table 2a Grid independence study for convection ($T_H = 1000$ K, $T_C = 300$ K, $Ra = 10^7$, $Pr_r = 0.71$)

Grid	Nu_H	Nu_C	Q_H (W)	Q_C (W)
14 × 14	19.29	15.41	354.32	283.06
18 × 14	19.01	16.25	349.11	298.40
22 × 14	18.83	16.93	345.90	311.00
26 × 14	18.74	17.46	344.23	320.69
30 × 14	18.70	17.79	343.46	326.74
34 × 14	18.65	17.96	342.47	329.88

Table 2b Grid independence study for convection–radiation interaction ($T_H = 1000$ K, $T_C = 300$ K, $Ra = 10^7$, $Pr_r = 0.71$, $\varepsilon = 0.1$)

Grid	Q_{conH} (W)	Q_{radH} (W)	Q_H (W)	Q_{conC} (W)	Q_{radC} (W)	Q_C (W)
14 × 14	272.13	189.05	461.18	297.58	143.38	440.96
18 × 14	272.22	189.70	461.81	314.12	142.75	456.87
22 × 14	273.82	190.26	464.08	328.66	142.22	470.88

been reported by the workers in this field. Only Leonardi and Reizes[4] reported similar observations. Also it is noted that the total heat transfer across the hot wall always exceeded the total heat transfer across the cold wall. This may be presumably due to the fact that the effect of variable property fluid (air, for the present case) is to inhibit convection near the hot wall since the viscosity of a gas increases with temperature; this results in a non-symmetric vertical velocity profile with stronger convection near the cold plate only. However, the thermal conductivity of gas also increases with temperature and this increase of gas conductivity dominates over the increase of gas viscosity. Consequently, the heat flux at hot wall increases. On the other hand, if a coarse mesh is adopted for computation of heat flux at the cold wall, which is associated with a strong convective flow field, an under-prediction of the cold wall heat flux value will result. Hence, it is expected that with refinement of grid sizes, the difference between the energy balances at the hot and cold wall should decrease. *Table 1a* confirms this observation. In *Table 2a* the results of the same experiment have been reported except the fact that the hot wall temperature has been exactly doubled. The study has been terminated at a mesh size of (34 × 14) and it is seen that still further refinement of mesh is necessary for obtaining even a fair agreement between the energy transfers at the active walls.

In the second phase of the grid independence study, the effect of both variable property convection and surface radiation has been considered. *Tables 1b* and *2b* show the detail of such a study. The energy balance along an active wall, in the present case, includes the net radiative transfer at the active walls in addition to the contribution from the convection. The salient features are as follows:

(1) the radiative contribution at either of the active walls do not vary much within the frame work of the present study. This may be attributed to the fact that since the fluid is not participating, the mesh refinement is not expected to exercise any significant influence upon it excepting the fact that there will be very small changes in the view factor calculations and this is reflected in the radiative contributions in terms of very small variations.

(2) In *Table 1a*, the terminal temperature difference is only 200 K; consequently the radiative contribution is only about 15% of its convective counterpart. As a result, convective heat transfer at the hot wall always exceeded that at the cold wall—a typical characteristic of pure variable property convection. In *Table 2b*, as the terminal temperature difference is increased to 700 K,

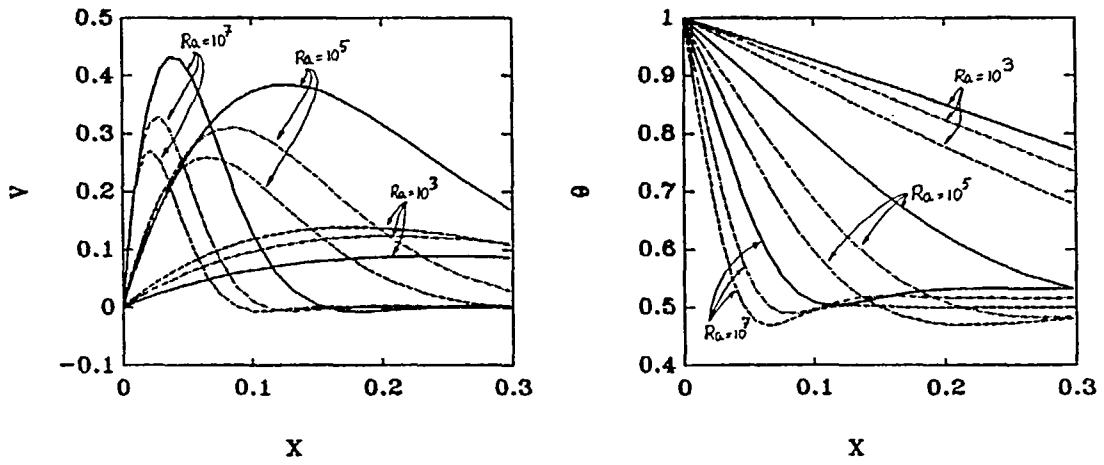

Figure 2 Mid-plane velocity and temperature distribution for convection. ——, TTD = 700 K; – · –, TTD = 200 K; ——, Boussinesq approximation

radiative contribution matches the order of convective contribution and it is noted that the convective transfer at the hot wall, for any mesh, is less than that at the cold wall, the reason for which will be described subsequently.

So it seems that better results can be obtained with a refined mesh for a pure convection study while relatively coarse mesh seems to be adequate for analysing the combined mode of transport. However, in the remaining part of this section, only the results, as obtained from a (30 × 14) mesh will be cited.

Effect of variable property natural convection

The effect of variable property natural convection on flow and temperature fields and comparisons is made with the incompressible flow situations, as and when possible.

Figure 2 describes the near wall vertical velocity distributions at $Y = 0.5$, for a range of Rayleigh numbers. It is observed that as the terminal temperature difference is gradually increased, the magnitude of the maximum vertical velocity increases; also the position of the maximum vertical velocity gradually moves away from the hot wall into the core. In the vicinity of the hot wall the vertical velocities, resulting from the constant property flow, are more than the vertical velocities from the compressible flow situations. This is expected since in the near wall region, the effect of gas viscosity is more pronounced. However, at some distance away from the hot wall, the effect of viscosity is less strongly felt and peaky velocity profiles are obtained. These observations are in good agreement with the observations of Shang and Wang[8], who have carried out an analytical investigation of variable property fluid flow along a vertical isothermal wall immersed in an infinite medium. On the contrary, Zhong *et al.*[6] concluded that the vertical velocity components (at $Y = 0.5$) for a variable property fluid are always smaller than those resulting from Boussinesq approximation. This observation by Zhong *et al.*[6] leads to the conclusion that as the terminal temperature difference is gradually increased, the convective motion gets suppressed throughout the cavity and in the limit, if radiation is not considered, heat transfer will be governed by conduction. This is rather difficult to accept since higher terminal temperature differences are associated with larger values of Grashoff number and consequently a stronger convection should result. *Figure 2* also describes the near wall temperature distributions at $Y = 0.5$ for some selected Rayleigh numbers. Because of the effect

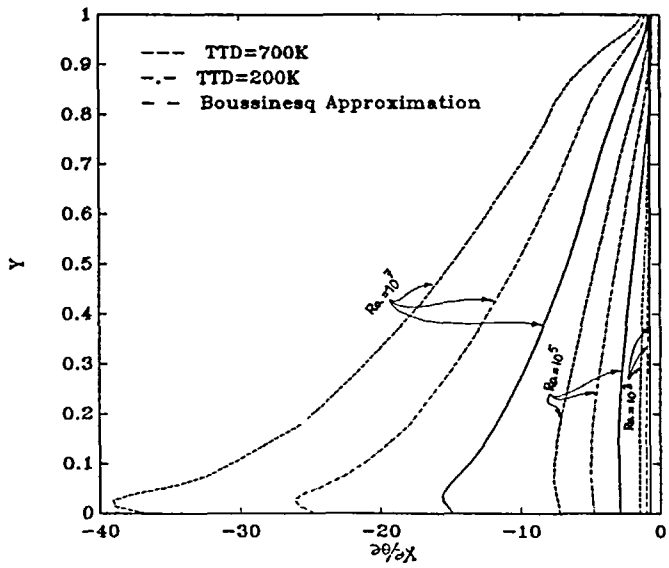

Figure 3 Distribution of $\partial\theta/\partial X$ along the hot wall (for convection)

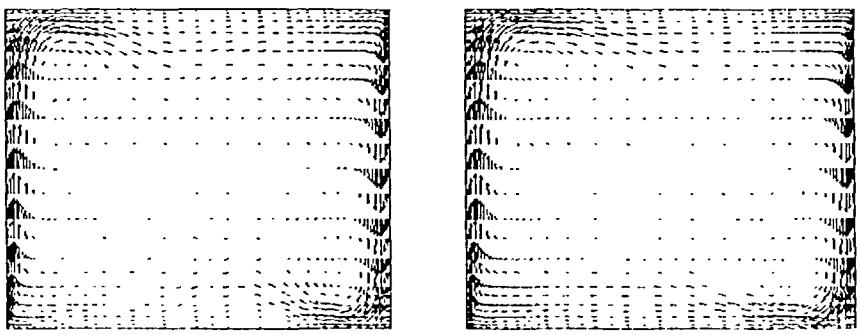

Figure 4 Velocity plot for convection and convection–radiation at $Ra = 10^7$ ($T_H = 500$ K, $T_C = 300$ K, $\varepsilon = 0.1$)

of gas viscosity, the effect of convection is somewhat suppressed with the result that as T_H is gradually increased over T_C, the temperature distributions become progressively flatter with respect to its counterpart with constant property fluid, i.e., higher the terminal temperature difference, the smaller will be the value of the temperature gradient (i.e. $\partial\theta/\partial X$). However, so far as convective heat transfer from the hot wall is concerned, the value of thermal conductivity at the hot wall increases with increase of T_H so that even though the temperature gradient is small, the convective heat transfer increases over constant property calculations. *Figure 3* describes some typical distributions of temperature gradients along the hot wall. As expected, maximum heat transfer occurs at the bottom of the hot wall.

Effect of interaction between convection and surface radiation

This section deals with the flow structure and isotherm patterns for the combined mode of heat transfer. *Figures 4–9* show the vector plot for velocities as well as temperature distributions

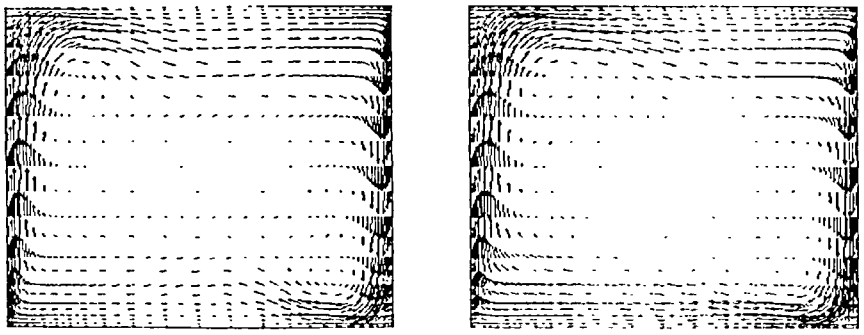

Figure 5 Velocity plot for convection and convection–radiation at $Ra = 10^7$ ($T_H = 1000$ K, $T_C = 300$ K, $\varepsilon = 0.1$)

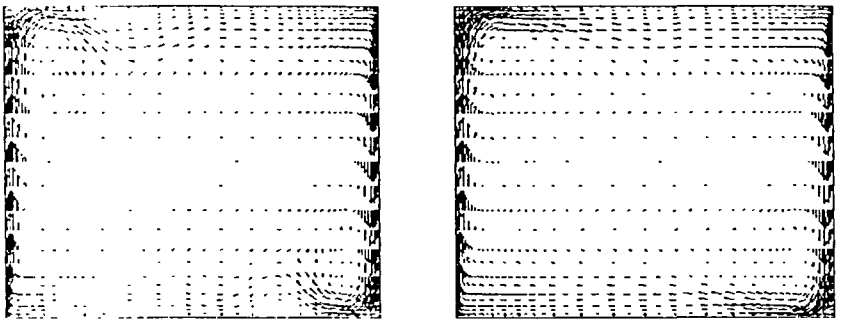

Figure 6 Velocity plot for convection and convection–radiation at $Ra = 4 \times 10^7$ ($T_H = 500$ K, $T_C = 300$ K, $\varepsilon = 0.1$)

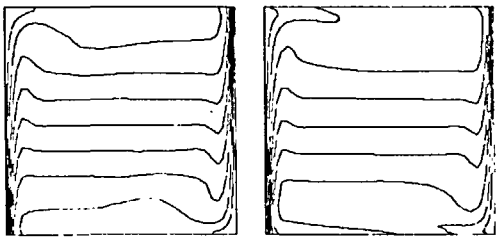

Figure 7 Isotherms for convection and convection–radiation at $Ra = 10^7$ ($T_H = 5000$ K, $T_C = 300$ K, $\varepsilon = 0.1$)

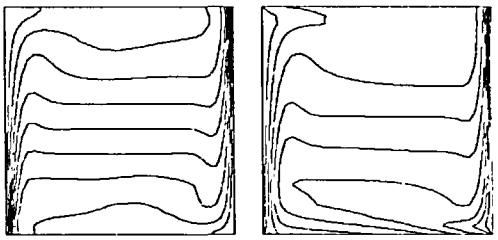

Figure 8 Isotherms for convection and convection–radiation at $Ra = 10^7$ ($T_H = 1000$ K, $T_C = 300$ K, $\varepsilon = 0.1$)

within the cavity in presence of convection and convection–radiation, for some selected Rayleigh numbers. Throughout the study, the value of ε has been assumed to be 0.1. Several important changes in flow pattern are apparent from these vector plots. For example, a pure convection case, based on variable property formulation, is characterized by the presence of multi-cells while the effect of radiation is to reduce their size or altogether eliminate them. Secondly, while there is a tendency towards the formation of separation cells at top and bottom horizontal plates for $Ra_H \geqslant 10^7$, such trends are completely absent in the presence of radiation. However, as the terminal temperature difference are decreased, the effect of radiation decreases and these trends reappear. The isotherm patterns, described in *Figures 7–9*, indicate that the effect of radiation is

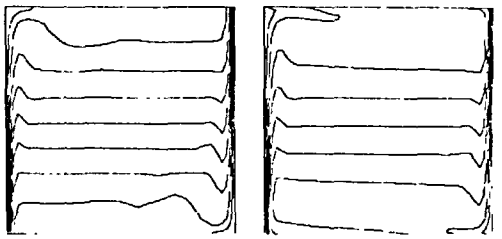

Figure 9 Isotherms for convection and convection–radiation at $Ra = 4 \times 10^7$ ($T_H = 500$ K, $T_C = 300$ K, $\varepsilon = 0.1$)

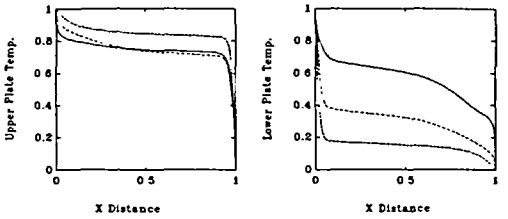

Figure 10 Upper and lower plate temperature distribution ($Ra = 10^7$). ---, TTD = 700 K (convection–radiation); -·-, TTD = 200 K (convection–radiation); ——, Boussinesq approximation (convection only)

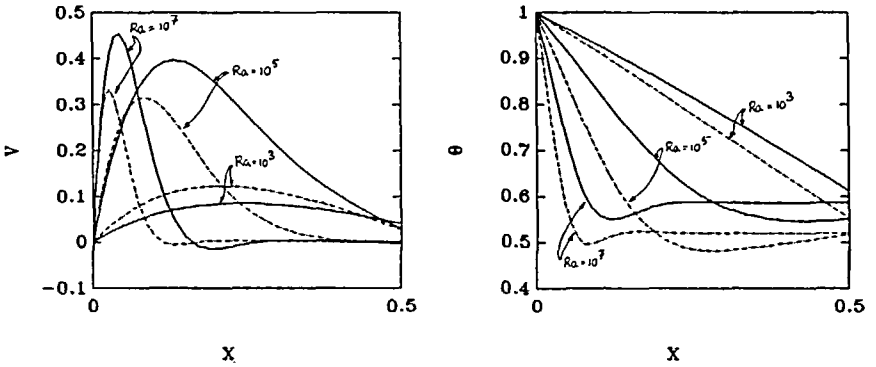

Figure 11 Mid-plane velocity and temperature distribution for convection–radiation. ---, TTD = 700 K; -·-, TTD = 200 K

to reduce the stratification in the core. Also it is seen that unlike the pure convection case, the insulated wall condition at the top and bottom are achieved through a balance of convective heat transfer and the radiative heat transfer at these walls; consequently, some typical isotherms are inclined to these walls. However, in all cases, where radiation is present, the bottom plate is being convectively cooled while the upper plate is convectively heated. Moreover, radiation weakens the convective field near the hot wall and this is readily evident by the spreading of isotherms in the vicinity of the hot wall. In general the isotherm patterns in these Figures agree well with the numerical investigations reported in Reference 14. *Figure 10* shows the temperature distributions along the upper and lower plates respectively. In this Figure, the sharp changes in temperature profiles are associated with the crowding of isotherms at the active walls. Also it is seen that the average plate temperature, in the presence of surface radiation, decreases below that of pure convection case for the upper plate while the reverse situation occurs for the lower plate; consequently, as the terminal temperature difference is increased gradually, the average temperature of the two plates approach each other. Moreover, the average temperature for the upper plate is affected to much lesser extent than the average temperature of the lower plate as the terminal temperature difference is increased.

Like the pure variable property convection case, it will be of interest to examine the mid-plane vertical velocity and temperature distribution when the radiation is present in addition to variable property convection. In *Figure 11*, these distribution patterns bear some similarity with *Figure 2* of particular interest is the mid-plane temperature distributions which show that at all the Rayleigh numbers considered in the present work, the core becomes intensively heated as terminal temperature difference is increased.

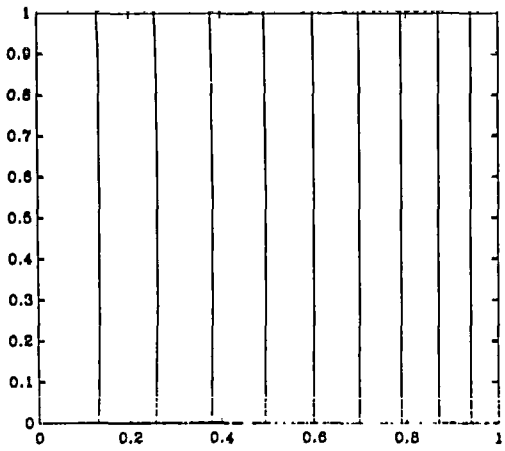

Figure 12 Isotherms for low convection regime (TTD = 700 K, $Ra = 0.1$, $\varepsilon = 0.1$)

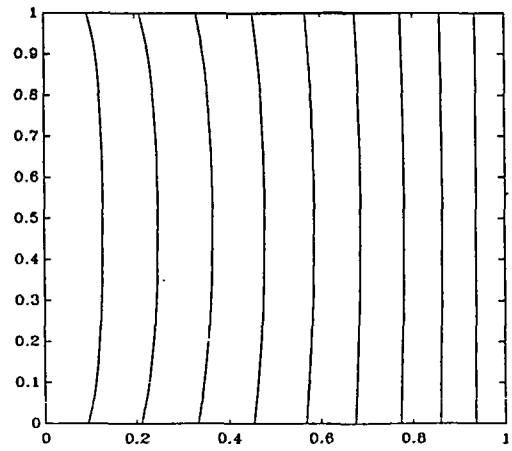

Figure 13 Isotherms for low convection regime (TTD = 700 K, $Ra = 0.1$, $\varepsilon = 0.8$)

Effect of interaction between variable property conduction and surface radiation

The isotherm patterns for the combined mode of variable property conduction and surface radiation with different surface emissivities are described. As can be seen from the system equations (2a)–(2d), it is not possible to shed the effect of natural convection completely; as a consequence the field behaviour for surface radiation and conduction is approached by making the Rayleigh number very small ($Ra = 0.1$). These sort of situations arise in practice when the cavity has very small dimension or when the experiment is carried out under microcavity condition. *Figures 12* and *13* illustrate the situations obtained by setting $Ra = 0.1$. In *Figure 12*, in which the surface emissivity was 0.1, radiation is expected to exert little influence. However, the effect of temperature dependent conductivity is clearly demonstrated. The isotherms are almost vertical indicating that the heat transfer mode is conduction dominated. However, the Figure reveals that the isotherms are not equispaced, which is a characteristic of constant thermal conductivity based conduction. As can be seen the isotherms near the hot wall are widely spaced while there is a packing of isotherms near the cold wall. This particular characteristic is explained by the fact that near the hot wall thermal conductivity is much higher. On the contrary, thermal conductivity near the cold wall is low necessitating the closer packing of isotherms near the cold wall. The effect of surface radiation on this conductive field is illustrated in *Figure 13*. As can be seen the isotherms near the hot wall show distinct departure from the conduction based results. The isotherms are curved in the vicinity of both the insulated walls while the central portion of the isotherms continued to retain their original character. It is natural to expect that the portions of the insulated walls near the hot wall assume major role in the radiative exchange process. The right hand side of (3), which governs the shape of the isotherms near the horizontal walls, then act as a perturbation over the conduction based pattern of isotherms. This explains the near wall curvature of the isotherms. This trend, however, is absent with the isotherms placed farthest from the hot wall since the portions of horizontal walls near the cold plate do not assume any significant role in radiation.

CONCLUSION

The present work deals with the finite element simulation of the interaction between variable property natural convection and surface radiation in a differentially heated square cavity. It has

been observed that the effect of radiation is to suppress the formation of multi-cells within the core, as well as the separation cells at the top and bottom plates. The core is intensively heated in presence of radiation and the thermal stratification of the core, which is a unique feature of both variable property and constant property convections, is lost. Moreover, isotherms are spread considerably apart near the hot wall when radiation is present. So far as variable property convection is concerned, the symmetry of the mid-plane vertical velocity and temperature profiles have been lost and the core is effectively reduced in size. From the numerical viewpoint, the presence of radiation considerably delays the convergence.

REFERENCES

1 de Vahl Davis, G. Natural convection of air in a square cavity, a bench mark numerical solution, *Int. J. Num. Meth. Fluids*, **3**, 249–264 (1983)
2 Polezhaev, V. I. Numerical solution of a system of two dimensional unsteady Navier–Stokes equation for a compressible gas in a closed region, *Fluid Dynam.*, **2**, 70–74 (1967)
3 Macgregor, R. K. and Emery, A. F. Free convection through vertical plane layers—moderate and high Prandtl number fluids, *ASME J. Heat Transfer*, **91**, 391–403 (1969)
4 Leonardi, E. and Reizes, J. A. Natural convection in compressible fluids with variable properties, *Proc. Ist Int. Conf. Num. Meth. Thermal Problems*, Pineridge Press, Swansea, pp. 297–306 (1979)
5 Leonardi, E. and Reizes, J. A. Natural convection heat transfer for variable property fluids using the Boussinesq approximation, *Proc. 2nd Int. Conf. Num. Meth. Thermal Problems*, Pineridge Press, Swansea, pp. 978–989 (1981)
6 Zhong, Z. Y., Yang, K. T. and Lloyd, J. R. Variable property effects in laminar natural convection in a square enclosure, *ASME J. Heat Transfer*, **107**, 133–138 (1985)
7 Shang, D. Y. and Wang, B. X. Effect of variable thermophysical properties on laminar free convection of gas, *Int. J. Heat Mass Transfer*, **33**, 1387–1395 (1990)
8 Shang, D. Y. and Wang, B. X. Effect of variable thermophysical properties on laminar free convection of polyatomic gas, *Int. J. Heat Mass Transfer*, **34**, 749–755 (1991)
9 Larson, D. W. and Viskanta, R. Transient combined laminar free convection and radiation in a rectangular enclosure, *J. Fluid Mech.*, **78**, 65–85 (1976)
10 Larson, D. W. Enclosed radiation and turbulent natural convection induced by a fire, *Numerical Methods in Heat Transfer*, Wiley, New York, pp. 467–487 (1981)
11 Lloyd, J. R., Yang, K. T. and Lin, V. K. A numerical study of one dimensional surface, gas and soot radiation for turbulent buoyant flows in enclosures, *Proc. Natl. Conf. Numer. Meth. Heat Transfer*, pp. 142–161 (1979)
12 Chang, L. C., Yang, K. T. and Lloyd, J. R. Radiation natural convection interactions in two dimensional complex enclosures, *J. Heat Transfer*, **105**, 89–95 (1983)
13 Louriat, G. A numerical study of a thermal insulation enclosure: influence of the radiative heat transfer, *19th Natl. Heat Transfer Conf., ASME Publ. HTD*, Vol 8, pp. 63–71 (1980)
14 Behnia, M., Reizes, J. A. and de Vahl Davis, G. Combined radiation and natural convection in a rectangular cavity with a transparent wall and containing a non-participating fluid, *Int. J. Num. Meth. Fluids*, **10**, 305–325 (1990)
15 Ozisik, M. N. *Heat Transfer, a Basic Approach*, McGraw-Hill, New York (1985)
16 Sarkar, A. and Sastri, V. M. K. Finite element solution of steady, two dimensional, natural convection equations, *Proc. Num. Meth. Thermal Problems*, Vol 2, Pineridge Press, Swansea, pp. 1732–1742 (1989)